18th Brazilian Congress of Thermal Sciences and Engineering
November 16-20, 2020 (Online)

ENC-2020-0426
NUMERICAL SOLUTION OF INTERNAL FLOW THROUGH A DE LAVAL NOZZLE BASED ON THE EULER MODEL WITH THE SU2 CODE: VERIFICATION AND VALIDATION

Giovanne Deni Iorio
Postgraduate Program in Mechanical Engineering (PGMEC), Federal University of Paraná (UFPR), Curitiba, PR, Brazil
giovanne.iorio@ufpr.br

Guilherme Bertoldo
Department of Physics, Statistics and Mathematics (DAFEM), Federal University of Technology – Paraná (UTFPR), Campus Francisco Beltrão, ZIP Code 85601-970, Francisco Beltrão, PR, Brazil
gbertoldo@utfpr.edu.br

Carlos Henrique Marchi
Laboratory of Numerical Experimentation (LENA), Department of Mechanical Engineering (DEMEC), Federal University of Paraná (UFPR), P.O. Box 19040, ZIP Code 81531-980, Curitiba, PR, Brazil
chmcfd@gmail.com

Abstract. *The present work performs the verification of the numerical solution of the internal flow through a de Laval nozzle obtained with the SU2 code and the validation of Euler's mathematical model. The flow was solved numerically in several meshes, where the finest one had 2048x1024 volumes. The discharge coefficient is the variable of interest, a coefficient that characterizes the flow and pressure losses. Comparisons of the numerical discharge coefficient with analytical and experimental results showed relative differences of 0.0257% and 0.379%, respectively, for the most refined simulated mesh. Comparisons also were made with the numerical solution of another computational code, finding relative differences of 0.000185%. Estimates of the numerical error were calculated based on error estimators. According to the GCI estimator, the numerical uncertainty does not exceed 0.001% of the numerical solution in the finest simulated mesh. Extrapolated solutions with Repeated Richardson Extrapolation and the convergent solution are also presented.*

Keywords: *nozzle, verification, validation, CFD, SU2*

1. INTRODUCTION

Verification and validation (V&V) are procedures that make it possible to assess the accuracy and reliability of a numerical solution. The first is the process that quantifies the numerical error and the second is the process that quantifies the modeling error caused by the limitations of the mathematical models to represent the real phenomenon (Roache, 2009).

This work aims to verify the solution of Euler's numerical model implemented in the SU2 code (Economon et al., 2016) and to validate Euler's mathematical model in the solution of fluid flow through a de Laval nozzle. A conical nozzle with angles of 45º in the convergent section and 15º in the divergent section will be considered. This nozzle has experimental data published by Back et al. (1965). The variable of interest in this study will be the discharge coefficient, a coefficient that characterizes the flow and pressure losses.

According to the ASME V&V 20-2009 standard, the verification of the solution must be preceded by code verification. That is why Van der Weide and Economon (2019) applied the method of manufactured solutions to perform the code verification of SU2 (version 7.0.0) and concluded that the code is error-free. The process of verifying numerical solutions and validating models obtained/implemented by the SU2 code was addressed by other authors (Palacios et al., 2013; Economon et al., 2016; Gori et al., 2017; Becker and Granzoto, 2018; Mishra et al., 2019; Castro, 2019). However, V&V of the SU2 code is usually performed for the Navier-Stokes mathematical model or turbulence models and the errors or numerical error estimates of the solutions obtained are generally not presented. Of the studies cited, only in the works of Mishra et al. (2019) and Castro (2019) the numerical error or its estimate were presented. Even though the SU2 code shows certain accuracy for a particular application, it does not mean that the same accuracy will be achieved in another application. Thus, a numerical simulation code must be evaluated in the largest possible number of applications.

In the present work, the estimated numerical uncertainty for the variable of interest will be calculated using the GCI (Grid Convergence Index) estimator (Roache, 1994), using the convergent estimator (Marchi and Silva, 2002) and with the estimator based on the Repeated Richardson Extrapolation (RRE) (Martins, 2013). In addition, the numerical solutions will be extrapolated with RRE and with the convergent estimator (Marchi et al., 2013).

In the following section, the flow simulation method and a definition of the variable of interest are presented. The procedures used for mesh generation and verification and validation are also shown. Section 3 presents the main results. Finally, a conclusion to this work is presented.

2. METHODOLOGY

2.1 Flow simulation

The flow is considered inviscid, non-reactive, axisymmetric and modeled by Euler's equations, which can be represented by (Hirsch, 2007)

$$\frac{\partial \mathbf{U}}{\partial t} + \nabla\cdot\mathbf{F}^c(\mathbf{U}) = 0 \tag{1}$$

where $\mathbf{U}$ is the vector of conservative variables and $\mathbf{F}^c$ is the advective flux, given by

$$\mathbf{U} = \begin{Bmatrix} \rho \\ \rho\mathbf{v} \\ \rho E \end{Bmatrix}, \quad \mathbf{F}^c = \begin{Bmatrix} \rho\mathbf{v} \\ \rho\mathbf{v}\otimes\mathbf{v} + \bar{\mathbf{I}}p \\ \rho E\mathbf{v} + p\mathbf{v} \end{Bmatrix} \tag{2}$$

In Eq. (1) t is time and in Eq. (2) ρ is the density, $\mathbf{v}$ is the velocity vector, E is the total energy per unit mass and p is the pressure. Furthermore, $\bar{\mathbf{I}}$ is a 2x2 identity matrix and $\otimes$ represents the tensor product. In Euler's system of equations, the equations represent the conservation of mass, the conservation of momentum and the conservation of total energy. Euler’s equations have as dependent variables ρ, $\mathbf{v}$, p and E; one can close the system of equations by assuming a constitutive relationship or state equation for the fluid, for example

$$p = (\gamma - 1)\rho[E - 0.5(\mathbf{v}\cdot\mathbf{v})] \tag{3}$$

where γ is the ratio of specific heats. In the SU2 code, the discretization of the Euler’s equation is performed through the Finite Volume Method in a vertex-based mesh (Economon et al., 2016). The advective fluxes are evaluated at the midpoint of the edges.

The discharge coefficient (C_d), which is the variable of interest in this work, characterizes the flow and pressure losses and it is defined as the ratio between the actual mass flow rate ($\dot{m}$) and the ideal mass flow rate ($\dot{m}_{ideal}$) (Anderson Junior, 2003) of the combustion gases. The equations of the ideal mass flow rate and the actual mass flow rate are shown in Eq. (4) and Eq. (5), respectively.

$$\dot{m}_{ideal} = p_0 A_t \sqrt{\frac{\gamma}{RT_0}\left(\frac{2}{\gamma + 1}\right)^{\frac{\gamma+1}{\gamma-1}}} \tag{4}$$

$$\dot{m} = \int_A \rho u dA \tag{5}$$

In Eq. (4), γ is the ratio of specific heats, R is the gas constant and A_t is the throat area. T_0 and p_0 are the temperature and pressure of stagnation. In Eq. (5), u is the axial component of the velocity vector, ρ is the density and A is the nozzle exit area. The integral present in Eq. (5) was numerically approximated using the Trapezoidal Rule.

In the simulations, the physical and geometric parameters of the Back et al. (1965) experiment with the nozzle BGM45-15 were considered, whose profile is illustrated in Fig. 1. Table 1 presents the flow parameters.

Table 1. Flow parameters.

Parameter	Value
Temperature of stagnation	833.333 K (1500 °R)
Pressure of stagnation	1725.068 kPa (250.2 psia)
External pressure	0 Pa
Ratio of specific heats	1.4
Gas constant	287.058 J/kg.K

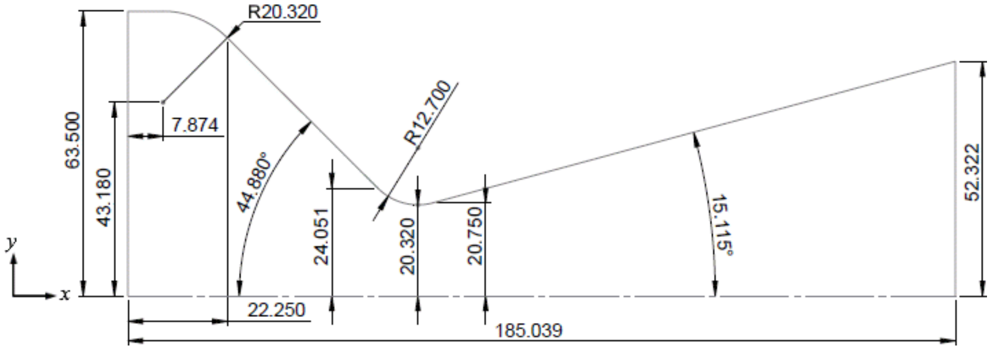

Figure 1. BGM45-15 nozzle profile with dimensions in millimeters.

The boundary conditions on the nozzle's wall is of adiabacity and impermeability, e.g.

$$\mathbf{n}\cdot\mathbf{v} = 0,\ \frac{\partial p}{\partial n} = 0,\ \frac{\partial T}{\partial n} = 0 \tag{6}$$

where T is the temperature and **n** is the normal vector. The first equation represents the fluid slipping condition, since the inviscid flow will be considered.

On the symmetry line, the radial velocity v is zero and adiabaticity and impermeability conditions are also considered for this boundary.

On the inlet of the nozzle, it is assumed that

$$\frac{\partial^2 u}{\partial x^2} = 0,\ \ v = 0 \tag{7}$$

where x is the axial direction. It is also considered that the inlet temperature and the inlet pressure are functions of the stagnation properties T_0 and p_0 presented in Tab. 1. These functions are given by (Sutton and Biblarz, 2016)

$$T = T_0[1 + \frac{1}{2}(\gamma - 1)M^2]^{-1} \tag{8}$$

$$p = p_0[1 + \frac{1}{2}(\gamma - 1)M^2]^{\frac{-\gamma}{\gamma - 1}} \tag{9}$$

where M is the Mach number and γ is the ratio of specific heats.

On the nozzle's outlet boundary, no boundary conditions are necessary, as the flow is supersonic, a situation in which the flow depends only on the upstream characteristics of the flow. However, numerically, a boundary condition is required, and the condition used is the extrapolation of the properties of the interior of the domain to the exit boundary.

For the simulations, the version 7.0.6 of the SU2 code with multiprocessing support for the Linux operating system was used. The simulations were performed in a computer with a processor Intel Core i5-9600K of 4.60 GHz and 16 GB of RAM memory.

2.2 Mesh generation

Non-orthogonal structured meshes were used in the simulations, which were generated using constant and simultaneous refinement ratio in the radial and axial directions. For the mesh generation, the code GMSH version 4.5.6 (Geuzaine and Remacle, 2009) for Linux was used.

The base mesh used in the simulations has 32 control volumes in the axial direction and 16 volumes in the radial direction. Figure 2 shows this base mesh. From this mesh, using a refinement ratio of two, six other meshes were generated. Thus, the following meshes were created: 32x16, 64x32, 128x64, 256x128, 512x256, 1024x512 and 2048x1024 volumes.

2.3 Errors and estimated errors

Numerical errors are always present in the flow solutions obtained through computational fluid dynamics (CFD). The main sources of these errors are: truncation errors E_h, round-off errors E_π and iteration errors E_i (Roache, 2009). In general, the numerical error E_n, present in the numerical solution of a generic variable of interest ϕ, can be symbolically represented by

$$E_n(\phi) = f(E_h, E_\pi, E_i) \tag{10}$$

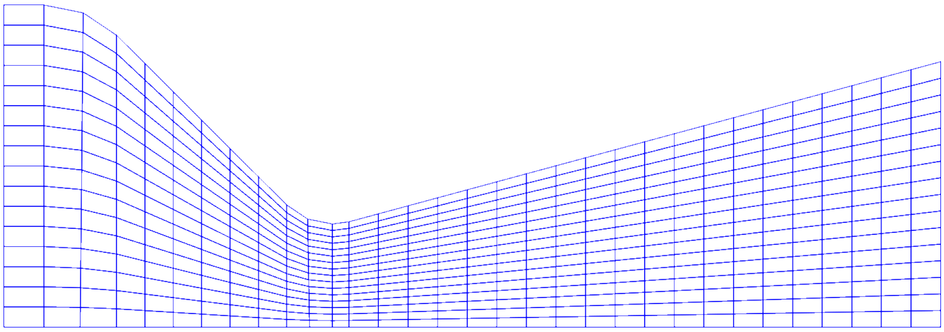

Figure 2. Base mesh with 32x16 volumes.

The numerical error can also be defined as the difference between the numerical solution ϕ and the exact analytical solution Φ of a variable of interest (Ferziger et al., 2020), i.e.,

$$E_n(\phi) = \Phi - \phi \tag{11}$$

In this work, care was taken to minimize round-off and iteration errors so that these errors could be considered negligible. Round-off errors were minimized by using double precision variables. Iteration errors were minimized by defining as a stop criterion of the iterative process as twice the number of iterations required for the residue of the mass conservation equation to be less than or equal to the tolerance of 10^{-14}. Hence, the numerical error of the numerical solution is represented only by the truncation error, that is,

$$E_h(\phi) = E_n(\phi) = \Phi - \phi \tag{12}$$

In this condition, the numerical error is denominated discretization error. Note that in practice, Φ is not known, so the numerical error must be estimated (U_n). Thereby,

$$U_n = \phi_\infty - \phi \tag{13}$$

where ϕ_∞ is an estimate of the exact solution.

The discretization error can be effectively estimated after obtaining the numerical solution. Some of the discretization error/uncertainty estimators are the GCI estimator (Roache, 1994), convergent estimator (Marchi and Silva, 2002) and RRE-based estimator (Martins, 2013). These estimators are used in this work.

In the verification process, the ASME V&V 20-2009 standard recommends performing the apparent order convergence analysis. As the mesh is refined, the apparent order p_U is expected to tend to the asymptotic order p_0 of the discretization error of the equations that model the problem. Divergences may indicate that other error sources are being generated by the code, inappropriate boundary conditions or incorrect initial conditions. In this study, it is expected that p_U converges to two. p_U is calculated with Eq. (14), where ϕ_{SC} is the solution obtained in a supercoarse mesh, ϕ_C is the solution obtained in a coarse mesh and ϕ_F is the solution obtained in a fine mesh and r is the refinement ratio.

$$p_U = \frac{log\left(\left|\frac{\phi_C - \phi_{SC}}{\phi_F - \phi_C}\right|\right)}{log(r)} \tag{14}$$

According to the ASME V&V 20-2009 standard, in addition to the numerical error E_n, a numerical solution ϕ is also subject to the modeling errors E_{model} and errors due to the uncertainty of the input data of the simulation (E_{input}). The modeling error is expected to be contained in the range given by

$$(E \pm U_{val}) \tag{15}$$

in other words,

$$E_{model} \in [E - U_{val}, E + U_{val}] \tag{16}$$

In Eq. (15) and Eq. (16), the symbols E and U_{val} are defined by the ASME V&V 20-2009 standard as validation metrics. The former is denominated comparison error and it is given by the difference between the numerical solution ϕ and the experimental result X. U_{val}, the validation standard uncertainty, can be calculated as

$$U_{val} = \sqrt{U_{num}^2 + U_{input}^2 + U_{exp}^2} \tag{17}$$

where U_{num}, U_{input} and U_{exp} are estimates of the standard numerical uncertainty, the standard uncertainty of the simulation input data and the standard uncertainty of the experimental error, respectively. Equation (17) is valid for cases where uncertainties are independent. The methodology for calculating U_{input} is presented in the ASME V&V 20-2009 standard. In addition, this standard relates U_{num} to the numerical error estimate of the GCI estimator (U_{GCI}) as follows

$$U_{num} = \frac{U_{GCI}}{k}, \quad 1.1 \leq k \leq 1.15 \tag{18}$$

Back et al. (1965) presented the experimental result (X) for the discharge coefficient (C_d). However, the experimental results were not tabulated in that study, being presented only in graphic form. Therefore, the code WebPlotDigitizer 4.2 (Marin et al., 2017) was used to extract the results from the graph. Hence, the value of the discharge coefficient obtained is

$$C_d = 0.9777 \pm 0.0056 \tag{19}$$

The uncertainty presented in the value of the experimental discharge coefficient encompasses both the experimental uncertainties and the uncertainty of reading the values in the graph.
Kliegel and Levine's (1969) analytical solution for the discharge coefficient, which assumes the flow as irrotational and isentropic, will be used for comparison with the values of the discharge coefficient obtained from the numerical simulations. For the problem treated in this work, the value obtained for the discharge coefficient by the method of Kliegel and Levine (1969) is

$$C_d = 0.981653876 \tag{20}$$

This value was calculated using quadruple precision.

The numerical solutions obtained in this present work will also be compared with the numerical discharge coefficient by Araki and Marchi (2017). Araki and Marchi (2017) studied the inviscid flow through the nozzle BGM45-15 and obtained the solution

$$C_d = 0.98140 \pm 0.00002 \tag{21}$$

for the ratio of specific heats 1.4.

3. RESULTS AND DISCUSSION

Table 2 presents the main results of the simulations. In this table, N_x is the number of volumes in the axial direction and N_y is the number of volumes in the radial direction. Moreover, "Iterations" indicates the number of iterations performed, "Time" represents the total simulation time, "RAM" means the maximum RAM memory consumption of each simulation, C_d is the discharge coefficient and p_U is the apparent order, calculated with Eq. (14). From this table, it is observed that the apparent order converges to two as the mesh is refined. Figure 3 shows the Mach number field obtained in the mesh m_7, which had a total of 2097152 volumes.

Table 2. General characteristics of the simulations.

Mesh	N_x	N_y	Iterations	Time	RAM (MB)	C_d	p_U
m_1	32	16	1436	1.49 s	113.92	1.01206217E+00	-
m_2	64	32	1844	5.56 s	120.19	9.88127628E-01	-
m_3	128	64	2538	30.73 s	148.87	9.83761632E-01	2.45
m_4	256	128	3398	4.20 min	249.24	9.82109643E-01	1.40
m_5	512	256	5354	31.06 min	635.93	9.81543049E-01	1.54
m_6	1024	512	10428	4.81 h	2176.48	9.81427137E-01	2.29
m_7	2048	1024	24535	1.91 day	8297.22	9.81401820E-01	2.19

Figure 3. Mach number field for the mesh with 2048x1024 volumes.

The discharge coefficient is presented with nine significant figures, as this is the maximum number of figures that was required in the final representation of the solutions with error estimation. In Roy and Oberkampf's (2011) framework for verification, validation and uncertainty quantification, two significant figures are used to report the error estimate and the solution is reported with the corresponding number of decimal places.

Table 3 shows comparisons between the numerical discharge coefficient and the analytical solution calculated by the method of Kliegel and Levine (1969). It is noticed that the absolute differences shown in Tab. 3 reduce with the mesh refinement, but from mesh m_6, the difference increases. This may have occurred because Kliegel and Levine's (1969) analytical solution does not necessarily represent the analytical solution of Euler's mathematical model since in its derivation the flow was considered irrotational and isentropic.

Table 3. Comparisons between numerical solutions and the irrotational and isentropic analytical solution of the discharge coefficient.

Case	C_d	Difference	Relative difference
m_1	1.01206217E+00	3.04E-02	3.10%
m_2	9.88127628E-01	6.47E-03	0.659%
m_3	9.83761632E-01	2.11E-03	0.215%
m_4	9.82109643E-01	4.56E-04	0.0464%
m_5	9.81543049E-01	1.11E-04	0.0113%
m_6	9.81427137E-01	2.27E-04	0.0231%
m_7	9.81401820E-01	2.52E-04	0.0257%
Convergent	9.81394063E-01	2.598E-04	0.02647%
RRE	9.81393831E-01	2.600E-04	0.02649%

The estimated numerical uncertainty/error of the numerical solution in the finest mesh obtained with the estimators GCI, convergent and RRE-based estimator, as well as the solutions extrapolated with the convergent solution and with RRE are presented in Tab. 4. Table 4 also shows the expression of the final solutions with the estimated numerical error. One can notice that the estimated error of the convergent solution and the solution extrapolated with RRE are, respectively, two and three orders of magnitude smaller than the estimated error obtained with the GCI estimator for the mesh m_7.

Table 4. Numerical discharge coefficient and its error/uncertainty estimation.

Method	C_d	Estimated error	Representation
GCI	9.81401820E-01	1.05E-05	0.981402 ± 0.000010
Convergent	9.81394063E-01	6.82E-07	0.98139406 ± 0.00000068
RRE	9.81393831E-01	4.82E-08	0.981393831 + 0.000000048

The solution obtained with the GCI method is close to that obtained by Araki and Marchi (2017) for the ratio of specific heats 1.4. Araki and Marchi (2017) obtained the solution 0.98140 ± 0.00002, also using a second order scheme and the Euler's mathematical model. They obtained this solution using a mesh with only 720x80 volumes; however, their numerical uncertainty is higher. Table 5 presents the comparisons between the numerical discharge coefficient obtained in this work and the Araki and Marchi's (2017) numerical solution. It can be noticed that the Araki and Marchi's (2017) solution range includes all the numerical solutions presented in Tab. 4. ASME V&V 20-2009 standard recommends comparing the numerical solution with ones obtained by other codes for the solution verification process. These kind of comparisons are denominated code-to-code comparison.

Table 5. Comparisons between numerical solutions and the Araki and Marchi's numerical solution.

Case	C_d	Difference	Relative difference
m_1	1.01206217E+00	3.07E-02	3.12%
m_2	9.88127628E-01	6.73E-03	0.686%
m_3	9.83761632E-01	2.36E-03	0.241%
m_4	9.82109643E-01	7.10E-04	0.0723%
m_5	9.81543049E-01	1.43E-04	0.0146%
m_6	9.81427137E-01	2.71E-05	0.00277%
m_7	9.81401820E-01	1.82E-06	0.000185%
Convergent	9.81394063E-01	5.94E-06	0.000605%
RRE	9.81393831E-01	6.17E-06	0.000629%

The comparisons between the numerical discharge coefficient and the experimental result obtained by Back et al. (1965) are presented in Tab. 6. In this case, the difference also reduces with the refinement of the mesh. The RRE solution has a smaller difference than the other ones.

Table 6. Comparisons between numerical solutions and the experimental result of the discharge coefficient.

Case	C_d	Comparison error	Relative difference
m_1	1.01206217E+00	3.44E-02	3.51%
m_2	9.88127628E-01	1.04E-02	1.07%
m_3	9.83761632E-01	6.06E-03	0.620%
m_4	9.82109643E-01	4.41E-03	0.451%
m_5	9.81543049E-01	3.84E-03	0.393%
m_6	9.81427137E-01	3.73E-03	0.381%
m_7	9.81401820E-01	3.70E-03	0.379%
Convergent	9.81394063E-01	3.6941E-03	0.37783%
RRE	9.81393831E-01	3.6938E-03	0.37781%

From Table 6, the validation metric E for the mesh m_7 is 0.0037. The validation standard uncertainty U_{val} for the most refined simulated mesh was calculated as

$$U_{val} = \sqrt{\left(\frac{U_{GCI}}{k}\right)^2 + U_{input}^2 + U_{exp}^2} = 0.0056 \quad (22)$$

where k equal to 1.1 was used and the U_{GCI} estimated numerical error for the mesh m_7 is shown in Tab. 4. U_{input} was calculated according to the methodology presented in ASME V&V 20-2009. The effects of temperature and pressure of stagnation were considered, and it resulted in U_{input} = 5.00E-16, indicating a low sensitivity of the discharge coefficient about these input parameters. It is noted that the predominant uncertainty in the validation standard uncertainty is the experimental uncertainty. As $|E| < U_{val}$, the combination of numerical, experimental and input data uncertainties is at the same order as the modeling error, i.e., the modeling error is within the noise level of the uncertainties, not allowing to evaluate whether the difference between the numerical solution and the experimental result is caused by the modeling error or other sources of error.

Figure 4 shows the pressure ratio distribution on the nozzle wall and at the symmetry line of the numerical solution of the mesh m_7. This figure also presents the pressure ratio distribution from the experimental wall pressures results of Back et al. (1965), which were presented only in graphic form by the authors, but whose values were extracted and tabulated by Radtke et al. (2013). As noted in Fig. 4, the numerical results of the wall pressure ratio are qualitatively similar to the experimental results, where the most significant differences are in the throat area.

The Mach number distribution on the nozzle wall and at the symmetry line are shown in Fig. 5. One can see an abrupt change in the Mach number in the symmetry line at position $x = 0.1476$. This is the position in which the shock wave meets the symmetry line, as seen in Fig. 3. The shock wave formed in this nozzle has experimental evidence given by Back and Cuffel (1966). According to the graph of pressure ratio distribution at the symmetry line presented by Back and Cuffel (1966), the position that the shock wave reaches the line of symmetry was calculated as $x = 0.1461 \pm 0.0017$, where the uncertainty considers the experimental pressure uncertainty and the uncertainty of reading the values in the graph. The abrupt change also happens for the other flow properties, as can be seen in Fig. 4 for the pressure ratio at the symmetry line and in Fig. 6 for the pressure field obtained in the mesh m_7. The temperature and density distributions are not shown in this work, as they have the same behavior as the pressure ratio.

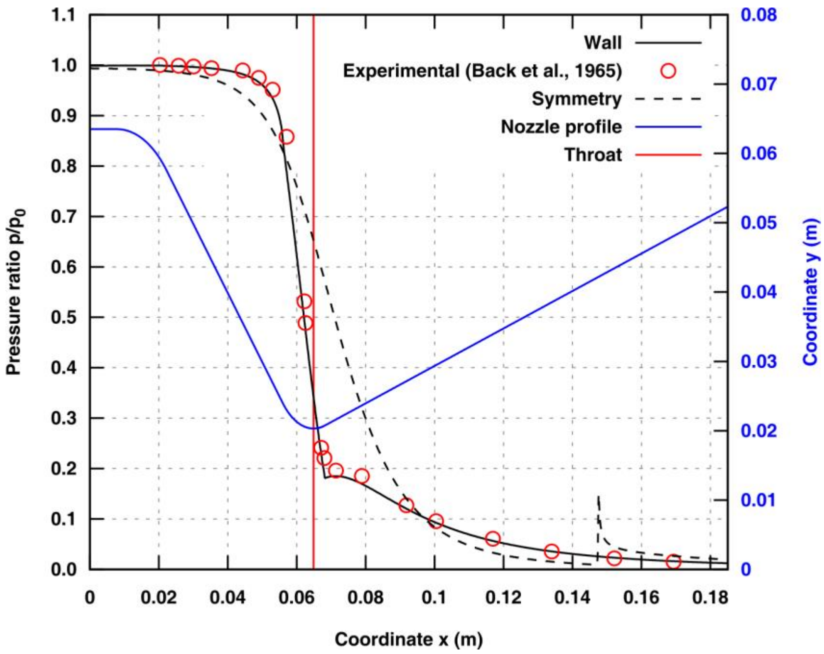

Figure 4. Comparison between the experimental and numerical results of the pressure ratio.

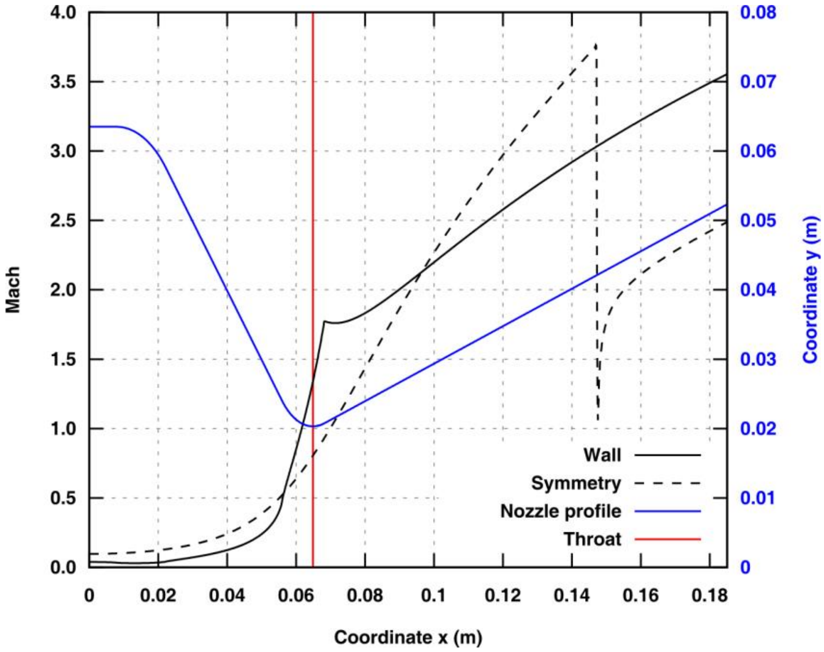

Figure 5. Numerical results of the Mach number on the nozzle wall and at the symmetry line.

Figure 6. Pressure field for the mesh with 2048x1024 volumes.

4. CONCLUSION

Comparisons between numerical discharge coefficients and analytical and experimental results were presented in this work and the differences showed reductions with mesh refinement. The relative differences for the most refined mesh simulated were 0.0257% in relation to the analytical result and 0.379% to the experimental result. The numerical solutions of the discharge coefficient also were compared to the numerical solution obtained by another computational code using the same mathematical model. In this case, the relative difference for the finest simulated mesh was 0.000185%. There was also a convergence of the apparent order to the asymptotic order, which is one of the code verification requirements proposed by the ASME V&V 20-2009 standard. It is estimated that the exact numerical solution for the discharge coefficient is contained in the range given by 0.981402 ± 0.000010. As for the modeling error, it is expected to be contained in the interval given by 0.38% ± 0.57% of the experimental result, where the first term is the comparison error and the second is the validation standard uncertainty, both divided by the experimental result of the discharge coefficient. In this case, the validation standard uncertainty is greater than the comparison error, indicating that the modeling error is within the noise level of the experimental, input and numerical uncertainties.

5. ACKNOWLEDGEMENTS

The authors acknowledge Postgraduate Program in Mechanical Engineering (PGMEC) of Federal University of Paraná (UFPR) and the Conselho Nacional de Desenvolvimento Científico e Tecnológico (CNPq) for physical and financial support given for this work. This study was financed in part by the Coordenação de Aperfeiçoamento de Pessoal de Nível Superior (CAPES), Finance Code 001. Carlos H. Marchi is supported by a CNPq scholarship. The first author also acknowledges Dener Augusto Iorio by assisting in the development and usage of the computational codes employed in this work.

6. REFERENCES

Anderson Junior, J. D., 2003. *Modern compressible flow: with historical perspective*. McGraw-Hill, New York, 3rd edition.

Araki, L. K. and Marchi, C. H., 2017. "Verification and validation of numerical solutions of two-dimensional reactive flow in rocket engine nozzles". *Applied Mathematical Modelling*, Vol. 52, pp. 544-557.

ASME V&V 20–2009, 2009. *Standard for Verification and Validation in Computational Fluid Dynamics and Heat Transfer*. ASME, New York, United States of America.

Back, L. H. and Cuffel, R. F., 1966. "Detection of oblique shocks in a conical nozzle with a circular-arc throat". *AIAA Journal*, Vol. 4, No. 12, pp. 2219-2221.

Back, L. H., Massier, P. F. and Gier, H. L., 1965. "Comparison of measured and predicted flows through conical supersonic nozzles, with emphasis on the transonic region". *AIAA Journal*, Vol. 3, No. 9, pp. 1606-1614.

Becker, G. G. and Granzoto, R. M., 2018. "DPW-6 and HiLiftPW-3 using the Stanford University Unstructured (SU2)". In *Proceedings of the 36th Applied Aerodynamics Conference* – AIAA Aviation Forum 2018. Atlanta, United States of America.

Castro, Í. C., 2019. *Assessment of SU2 for radial compressor performance prediction*. Master's thesis, Delft University of Technology, Delft, Netherlands.

Economon, T. D., Palacios, F., Copeland, S. R., Lukaczyk, T. W. and Alonso, J., 2016. "SU2: an open-source suite for multiphysics simulation and design". *AIAA Journal*, Vol. 54, No. 3, pp. 828-846.

Ferziger, J. H., Perić, M. and Street, R. L., 2020. *Computational methods for fluid dynamics*. Springer, Zug, 4th edition.

Geuzaine, C. and Remacle, J. F., 2009. "Gmsh: a three-dimensional finite element mesh generator with built-in pre- and post-processing facilities". *International Journal for Numerical Methods in Engineering*, Vol. 79, No. 11, pp. 1309-1331.

Gori, G., Zocca, M., Gammi, G., Spinelli, A. and Guardone, A., 2017. "Experimental assessment of the open-source SU2 CFD suite for ORC applications". *Energy Procedia*, Vol. 129, pp. 256-263.

Hirsch, C., 2007. *Numerical computation of internal and external flows: fundamentals of computational fluid dynamics*. Elsevier, Oxford, 2nd edition.

Kliegel, J. R. and Levine, J. N., 1969. "Transonic flow in small throat radius of curvature nozzles". *AIAA Journal*, Vol. 7, No. 7, pp. 1375-1378.

Marchi, C. H., Novak, L. A., Santiago, C. D. and Vargas, A. P. S, 2013. "Highly accurate numerical solutions with Repeated Richardson Extrapolation for 2D Laplace equation". *Applied Mathematical Modelling*, Vol. 37, No. 12-13, pp. 7386-7397.

Marchi, C. H. and Silva, A. F. C., 2002, "Unidimensional numerical solution error estimation for convergent apparent order". *Numerical Heat Transfer*, Part B, Vol. 42, No. 2, pp. 167-188.

Marin, F., Rohatgi, A. and Charlot, S., 2017. "WebPlotDigitizer, a polyvalent and free software to extract spectra from old astronomical publications: application to ultraviolet spectropolarimetry". *French Society of Astronomy & Astrophysics*.

Martins, M. A., 2013. *Multiextrapolação de Richardson com interpolação para reduzir e estimar o erro de discretização em CFD*. Ph.D. thesis, Universidade Federal do Paraná, Curitiba, Brazil.

Mishra, A. A., Mukhopadhaya, J., Iaccarino, G. and Alonso, J. J., 2019. "Uncertainty estimation of turbulence model predictions in SU2". *AIAA Journal*, Vol. 57, No. 3, pp. 1066-1077.

Palacios, F., Colonno, M. R., Aranake, A. C., Campos, A., Copeland, S. R., Economon, T. D., Lonkar, A. K., Lukaczyk, T. W., Taylor, T. W. R. and Alonso, J. J., 2013. "Stanford University Unstructured (SU2): an open-source integrated computational environment for multi-physics simulation and design". In *Proceedings of the 51st Aerospace Science Meeting including the New Horizons Forum and Aerospace Exposition* - AIAA Meeting Paper 2013. Grapevine, United States of America.

Radtke, J. J., Marchi, C. H., Araki, L. K., Bertoldo, G., Moro, D. F., Germer, E. M., 2013. "Verificação e validação da solução numérica do código Mach2D para problemas de propulsão de foguetes". In *Proceeding Series of the Brazilian Society of Computational and Applied Mathematics* - CMAC-SE 2013. Bauru, Brazil.

Roache, P. J., 1994. "Perspective: a method for uniform reporting of grid refinement studies". *ASME Journal of Fluids Engineering*, Vol. 116, No. 3, pp. 405-413.

Roache, P. J., 2009. *Fundamentals of verification and validation*. Hermosa, Albuquerque.

Roy, C. J. and Oberkampf, W. L., 2011. "A comprehensive framework for verification, validation, and uncertainty quantification in scientific computing". *Computer Methods in Applied Mechanics and Engineering*, Vol. 200, No. 25-28, pp. 2131-2144.

Sutton, G. P. and Biblarz, O., 2016. *Rocket propulsion elements*. John Wiley & Sons, Hoboken, 9th edition.

Van der Weide, E. and Economon, T. D., 2019. "Accuracy verification by means of exact and manufactured solutions". In *Proceedings of the 4th SU2 Developers Meeting* - SU2 Foundation 2019. Varenna, Italy.

7. RESPONSIBILITY NOTICE

The authors are the only responsible for the printed material included in this paper.